Available online at www.sciencedirect.com
ScienceDirect
J. Chem. Thermodynamics 39 (2007) 1539–1545
JCT
www.elsevier.com/locate/jct

Thermodynamic evidence for phase transition in $MoO_{2-\delta}$

K.T. Jacob [a,c,*], V.S. Saji [a], J. Gopalakrishnan [b], Y. Waseda [c]

[a] Department of Materials Engineering, Indian Institute of Science, Bangalore 560 012, India
[b] Solid State and Structural Chemistry Unit, Indian Institute of Science, Bangalore 560 012, India
[c] Institute of Multidisciplinary Research for Advanced Materials, Tohoku University, Aobaku, Sendai 980-8577, Japan

Received 30 May 2007; received in revised form 7 September 2007; accepted 12 September 2007
Available online 19 September 2007

Abstract

The standard Gibbs free energy of formation of $MoO_{2-\delta}$, $\Delta_f G^\circ(MoO_{2-\delta})$, has been measured over a wide temperature range (925 to 1925) K using an advanced version of bi-electrolyte solid-state electrochemical cell incorporating a buffer electrode:

$$Pt|Mo + MoO_{2-\delta}\| (Y_2O_3)ThO_2\| (CaO)ZrO_2\| O_2(0.1\ MPa)|Pt$$

The Gibbs free energy of formation of $MoO_{2-\delta}$, which is directly related to the measured cell e.m.f., can be represented by two linear segments:

$$\Delta_f G^\circ(MoO_{2-\delta}) \pm 570/(J\cdot mol^{-1}) = -579,821 + 170.003(T/K),$$

in the temperature range (925 to 1533) K, and

$$\Delta_f G^\circ(MoO_{2-\delta}) \pm 510/(J\cdot mol^{-1}) = -564,634 + 160.096(T/K),$$

in the temperature range (1533 to 1925) K. The change in slope at $T = 1533$ K is probably related to the phase transition of MoO_2 from monoclinic structure with space group $P2_1/c$ to tetragonal structure characteristic of rutile with space group $P4_2/mnm$. The enthalpy and entropy change for the phase transition are: $\Delta H_{tr} = (15.19 \pm 2.1)\ kJ\cdot mol^{-1}$; $\Delta S_{tr} = (9.91 \pm 1.27)\ J\cdot mol^{-1}\cdot K^{-1}$. The standard enthalpy of formation of $MoO_{2-\delta}$ at $T = 298.15$ K assessed by the third-law method is: $\Delta_f H^\circ(MoO_{2-\delta}) = (-592.28 \pm 0.33)\ kJ\cdot mol^{-1}$. The new measurements refine thermodynamic data for MoO_2.

Keywords: MoO_2; Gibbs free energy of formation; Phase transition; E.m.f. measurement; Enthalpy of formation

1. Introduction

Mixture of high melting Mo and $MoO_{2-\delta}$ forms a convenient reference electrode in solid-state sensors for oxygen in liquid metals such as Fe, Ni, and Co. The sensors usually use stabilized-zirconia as a solid electrolyte. For the calibration of oxygen sensors, accurate data on Gibbs free energy of formation of $MoO_{2-\delta}$ is necessary. Gibbs free energy of formation of $MoO_{2-\delta}$ has been measured by a number of investigators using $CO + CO_2$ or $H_2 + H_2O$ gas-equilibrium [1–4] and oxide solid electrolyte techniques using a variety of reference electrodes [5–15]. However, there is considerable difference in reported results, part of which is caused by the uncertainty in the oxygen potential of the reference electrode. Ideally pure oxygen at standard pressure should be used to avoid this uncertainty. The particle size of the powders used was not specified in most of the studies reported in the literature. Jacob *et al.* [16] have shown that the e.m.f. of solid-state cells depend on particle size of the phases present at the electrodes when they are in the nanometer range. This study was aimed at resolving the uncertainty in thermodynamic data for MoO_2.

* Corresponding author. Address: Department of Materials Engineering, Indian Institute of Science, Bangalore 560 012, India. Tel.: +91 80 22932494; fax: +91 80 23600472.
E-mail address: katob@materials.iisc.ernet.in (K.T. Jacob).

0021-9614/$ - see front matter © 2007 Elsevier Ltd. All rights reserved.
doi:10.1016/j.jct.2007.09.005

In most of the earlier e.m.f. studies on $MoO_{2-\delta}$ zirconia-based solid electrolytes were used. Thoria-based electrolyte was employed in one study [14]. At high temperatures, the oxygen chemical potential at the $Mo + MoO_{2-\delta}$ electrode is close to the boundary for predominant ionic conduction (oxygen transport number >0.99) in stabilized-zirconia electrolytes [17,18]. Doped-thoria electrolyte, which retains ionic conduction at lower oxygen potentials, is a better choice. However, it develops hole conduction at high oxygen potentials. Hence, a combination of the two electrolytes is used, with yttria-doped thoria (YDT) near the $Mo + MoO_{2-\delta}$ electrode and calcia-stabilized zirconia (CSZ) near the oxygen electrode. The bi-electrolyte has a larger domain of ionic conduction than the individual electrolytes.

Even when the electrolyte operates in the predominantly ionic conduction domain, there is always some trace electronic or hole conductivity in the material [17–19]. The presence of trace electronic or hole conduction can give rise to a small electrochemical flux of oxygen from the high oxygen potential electrode to the low oxygen potential electrode. The electrochemical permeability is caused by the coupled transport of oxygen ions and holes/electrons in the solid electrolyte under the oxygen potential gradient. The oxygen flux can polarize the electrodes resulting in lower e.m.f. A buffer electrode, introduced between reference and working electrodes, can act as a sink for the oxygen flux and prevent the flux from reaching the working electrode.

In the present study, the standard Gibbs free energy of formation of $MoO_{2-\delta}$ was measured over a large temperature range (925 to 1925) K using a solid-state electrochemical cell incorporating both YDT and CSZ as electrolytes with pure oxygen as the reference electrode. An advanced cell design incorporating a buffer electrode was used. During the course of measurement, evidence for an important phase transition in $MoO_{2-\delta}$ was obtained in addition to accurate thermodynamic data. This phase transition has not been reported earlier and is therefore highlighted in this article.

2. Experimental

2.1. Materials

Puratronic grade Mo and MoO_2 powders were obtained from Johnson and Matthey Chemicals (Royson, United Kingdom). The oxide was fired at $T = 1373$ K in argon atmosphere and the metal was first reduced under pure dry hydrogen and then vacuum treated at the same temperature before use. The Mo–MoO_2 electrode was prepared by intimately mixing Mo and MoO_2 in equimolar ratio, compacting the mixture in a steel die at 150 MPa and sintering the resulting pellet at $T = 1673$ K for 72 h under pre-purified argon gas. The pellet was contained in an alumina crucible. A thin layer of the pellet in contact with the alumina crucible was removed by grinding to minimize contamination. The X-ray diffraction analysis (XRD) at room temperature indicated that MoO_2 was monoclinic with lattice parameters $a = 0.5609$ nm, $b = 0.4869$ nm, $c = 0.5626$ nm and $\beta = 120.91°$. SEM analysis showed that the particle size of the metal and oxide powders were in the range (4 to 13) μm. High-density impervious YDT and CSZ tubes and YDT powder were obtained from a commercial source. The CSZ tubes closed at one end were leak tested under vacuum before use.

2.2. Apparatus and procedure

The reversible e.m.f. of the following solid-state cell was measured as a function of temperature:

$$\mathrm{Pt|Mo + MoO_2 \| (Y_2O_3)ThO_2 \| (CaO)ZrO_2 \| O_2(0.1\,MPa)|Pt} \quad \text{(I)}$$

The cell is written such that the right-hand side electrode is positive. The reference electrode of pure oxygen at constant pressure is non-polarizable. The chemical potential of oxygen in the micro-system near the working electrode/electrolyte interface can be altered because of the semi-permeability of the electrolyte to oxygen. The oxygen flux arriving at the working electrode can increase the oxygen chemical potential at the interface and result in lower e.m.f. To prevent polarization of the measuring electrode, a buffer electrode is introduced between the reference and measuring electrodes separated by solid electrolytes as shown below:

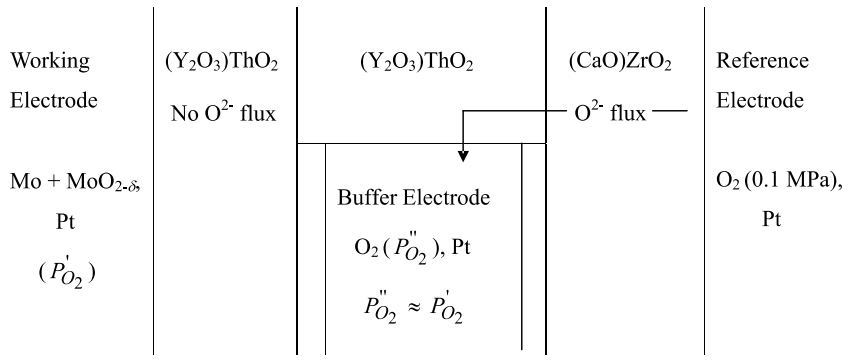

The buffer electrode absorbs the oxygen flux and prevents it from reaching the working electrode. To be effective, the buffer electrode should be maintained at an oxygen chemical potential close to that of the working electrode. Since there is no significant difference between the chemical potentials of buffer and working electrodes, driving force for transport of oxygen through the YDT electrolyte separating these electrodes does not exist. The working electrode therefore remains unpolarized. The e.m.f. of the cell is determined only by the oxygen chemical potentials at the reference and working electrodes, which are connected by oxygen ion conductors. Thus, the three-electrode design of the cell prevents error in e.m.f. caused by polarization of the working electrode. An amplified schematic of the oxygen potential variation through the cell is shown in figure 1. Measuring separately the e.m.f. between the three electrodes, two at a time, can assess the magnitude of the polarization effect as illustrated on the diagram. Transport of oxygen between the electrodes through the gas phase is prevented by physical isolation of the gas phase over the three electrodes.

The cell design used for high-temperature e.m.f. measurements at $T < 1473$ K is shown in figure 2. It consisted of three distinct electrode compartments. The reference electrode is contained inside an inverted impervious calcia-stabilized zirconia (CSZ) tube. The buffer electrode, consisting of $Mo + MoO_{2-\delta}$ is contained inside a CSZ crucible lined with a layer of yttria-doped thoria (YDT). An ionic bridge of YDT was provided through the buffer electrode, so that the reference and working electrodes are connected by a solid electrolyte combination through which only oxygen ions can be transported. The gas phase over the working electrode was separated from that over the buffer electrode by a tube of stabilized-zirconia spring loaded against the YDT pellet. The cell e.m.f. measured between the working and reference electrodes was determined only by the oxygen chemical potential at these electrodes and was not affected by the gradient of chemical potential through the connecting chain consisting of the solid electrolyte segments including the ionic bridge across the buffer electrode. Construction of the high-temperature galvanic cell was rendered more difficult by the introduction of the buffer electrode. The static vacuum-sealed cell construction used by Charette and Flengas [20] was adopted in this study in preference to other designs that employ either dynamic vacuum or inert gas flow over the electrodes [18,21] at $T < 1473$ K. Further details of the cell assembly and operational procedures used in this study can be found in earlier publications [22,23]. To prevent deformation of the quartz tube under vacuum, the cell enclosure was partially filled with high purity Ar gas when operated between $T = (1273$ and 1473 K).

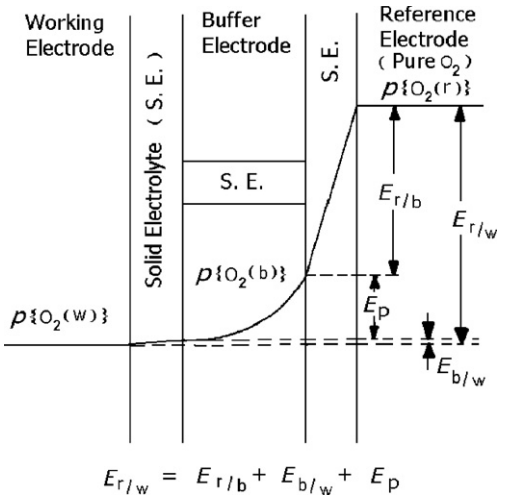

FIGURE 1. Oxygen chemical potential variation across the solid-state cell with a buffer electrode and the corresponding e.m.f. between electrode pairs.

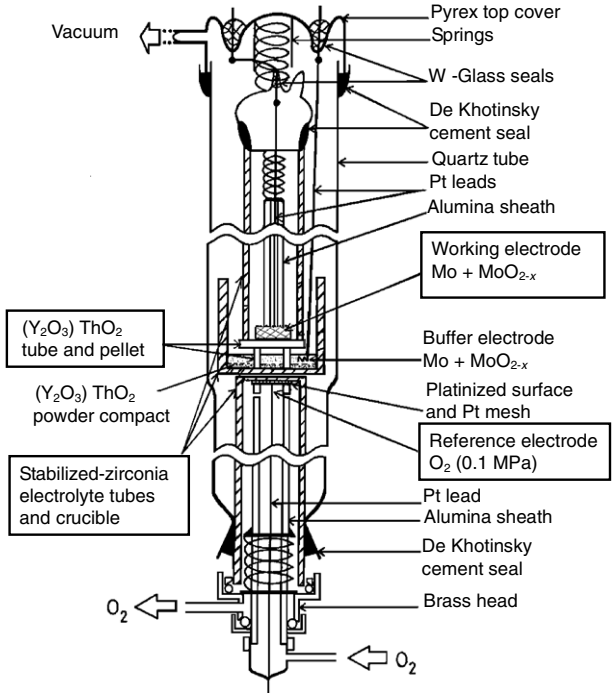

FIGURE 2. A schematic diagram of the cell assembly for $T/\mathrm{K} < 1473$.

In higher temperature range (1373 to 1925) K, an alumina tube fitted with water-cooled brass heads at the two ends is used to enclose the cell. Further, a vertical resistance furnace with molybdenum tape as the heating element was employed for generating the high temperatures. The tape was protected from oxidation by a flowing gas mixture containing 90% N_2 and 10% H_2. Since the alumina tube has a small permeability for gases (especially hydrogen and oxygen) at high temperatures, a double alumina tube enclosure was used. This arrangement is described in detail in the earlier publications [24,25]. The annular space between the two alumina tubes was purged with a stream of high purity Ar gas to prevent the ingress of hydrogen and oxygen into the cell environment. The cell was operated under flowing ($5\ \mathrm{ml} \cdot \mathrm{s}^{-1}$) inert gas. The pressure of Ar over the measuring and buffer electrodes was ~5000 Pa above atmospheric. The high-purity Ar gas was

dried and deoxidized before use. The Pt electrodes were replaced with Pt–20% Rh wire.

The e.m.f. of the solid-state electrochemical cell was measured at regular intervals between $T = (925$ and 1925) K with a high-impedance ($>10^{12}\ \Omega$) digital voltmeter. The reversibility of each cell was confirmed by micro-coulometric titration ($\sim$50 μA for 100 s) of oxygen in both directions. In each case, the e.m.f. was found to return gradually to its original value before titration. The e.m.f. was reproducible during heating and cooling cycles. At the end of each experiment, the electrodes were cooled to room temperature and examined by X-ray diffraction. There was no evidence of change in the phase assemblage of the electrodes during the experiment. The steady state e.m.f. was obtained in (1 to 6) ks, depending on the temperature of the measurement. By measuring the e.m.f. between the three electrodes, the polarization effect (E_p in figure 1) was found to vary from (6 to 12) mV depending on temperature. The e.m.f. between the buffer and working electrodes ($E_{b/w}$) was negligible, (±0.1) mV. The e.m.f. of the cell operated under vacuum and static Ar with silica enclosure was almost identical (±0.2) mV to the e.m.f. obtained with alumina enclosure and flowing Ar atmosphere in the overlapping temperature range.

3. Results and discussion

Figure 3 shows variation of the reversible e.m.f. of the cell as a function of temperature. The overall cell reaction is:

$$\mathrm{Mo(solid) + O_2(gas) \rightarrow MoO_2(solid)} \qquad (1)$$

The change in slope at $T = 1533$ K suggests a phase transition of $MoO_{2-\delta}$ with a relatively small entropy change. Additional evidence about the nature of this transition comes from thermodynamic and phase equilibrium studies on the system ($MoO_2 + TiO_2$) [26]. The solid solubility of TiO_2 in monoclinic MoO_2 is very restricted (less than 2.5 mol%) up to $T = 1412$ K. There is extended solid solubility above $T = 1533$ K and complete solid solubility above $T = 1560$ K. The solid solution with tetragonal structure exhibits a solid-state miscibility gap characterized by critical temperature $T^c = 1560$ K and composition $X^c_{TiO_2} = 0.38$. In the range $T = (1412$ to 1533 K) there is a two-phase region, involving monoclinic MoO_2 and solid solution with tetragonal structure, which terminates at the eutectoid reaction at $T^R = 1412$ K and $X^R_{TiO_2} = 0.17$. Since structural compatibility between end members is an essential requirement for forming a continuous range of solid solution, it may be safely concluded that the structure of MoO_2 at high temperature must be identical to that of TiO_2 (rutile). In view of this additional evidence, the phase transition identified in this study can be described as that of $MoO_{2-\delta}$ from monoclinic structure with space group $P2_1/c$ to tetragonal structure with space group $P4_2/mnm$. Although the high-temperature form of MoO_2 could not be quenched to room temperature, ($MoO_2 + TiO_2$) solid solutions with tetragonal structure can be quenched. By extrapolating the lattice parameters of the solid solution, the lattice constants of monoclinic MoO_2 were evaluated: $a = 0.4850$ nm and $c = 0.2812$ nm [26].

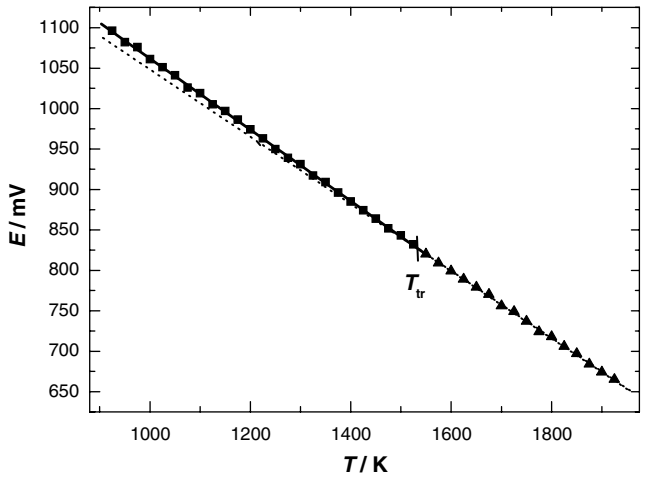

FIGURE 3. Measured e.m.f., E of the solid-state cell as a function of temperature T.

The least-squares regression analysis of the e.m.f. of the cell in the temperature range (925 to 1533) K gives:

$$E \pm 1.48/(\mathrm{mV}) = 1502.36 - 0.44049(T/\mathrm{K}), \qquad (2)$$

where the uncertainty limit corresponds to the standard deviation obtained from regression analysis. In the temperature range (1533 to 1925) K, e.m.f. variation is given by:

$$E \pm 1.32/(\mathrm{mV}) = 1463.01 - 0.41482(T/\mathrm{K}). \qquad (3)$$

The measured e.m.f. of the cell is related to the standard Gibbs free energy change associated with the cell reaction by the Nernst equation; $\Delta_f G^\circ = -nFE$, where $n = 4$ is the number of electrons involved in the electrode reactions, $F/\mathrm{J \cdot V^{-1}} = 96{,}485$ is the Faraday constant and E/V is the measured e.m.f. of the cell. The standard Gibbs free energy of formation of $MoO_{2-\delta}$ with monoclinic structure in the temperature range (925 to 1533) K can be represented by the expression:

$$\Delta_f G^\circ(MoO_{2-\delta}) \pm 570/(\mathrm{J \cdot mol^{-1}}) = -579{,}821 + 170.003(T/\mathrm{K}). \qquad (4)$$

For $MoO_{2-\delta}$ with tetragonal structure in the temperature range (1533 to 1925) K:

$$\Delta_f G^\circ(MoO_{2-\delta}) \pm 510/(\mathrm{J \cdot mol^{-1}}) = -564{,}634 + 160.096(T/\mathrm{K}). \qquad (5)$$

The temperature-independent terms in equations (4) and (5) are the enthalpies of formation of the two forms of MoO_2 at an average temperature in the range of measurement. The temperature-dependant terms are related to the corresponding entropies of formation.

Table 1 summarizes all the information available in the literature on the Gibbs free energy of formation of MoO_2,

TABLE 1
Comparison of experimental information and Gibbs free energies of formation of $MoO_{2-\delta}$, $\Delta_f G^\circ(MoO_{2-\delta})$

Year	Investigators	Technique/reference electrode	Temperature range, T/K	$\Delta_f G^\circ/(kJ \cdot mol^{-1})$
1940	Tonosaki [1]	H_2/H_2O	918 to 1096	$-550.199 + 0.1457T$
1953	Gokcen [2]	H_2/H_2O	950 to 1330	$-553.334 + 0.1469T$
1962	Gleiser and Chipman [3]	CO/CO_2	1200 to 1350	$-576.932 + 0.1681T$
1963	Rapp [5]	e.m.f./Fe + "FeO" and Ni + NiO	1020 to 1320	$-575.300 + 0.1674T$
1964	Barbi [6]	e.m.f./"FeO" + Fe_3O_4 and Fe + Fe_3O_4	840 to 1100	$-575.856 + 0.1778T$
1965	Drobyshev *et al.* [7]	e.m.f./Fe + "FeO"	1260 to 1360	$-575.635 + 0.1697T$
1968	Vassilev *et al.* [4]	H_2/H_2O	773 to 1123	$-533.887 + 0.1336T$
1969	Berglund and Kierkegaard [8]	e.m.f./air	1150 to 1450	$-564.798 + 0.161T$
1972	Alcock and Chan [9]	e.m.f./CO/CO_2	1273 to 1873	$-579.902 + 0.1674T$
1979	Iwase *et al.* [10]	e.m.f./Co + CoO and air	1223 to 1723	$-576.100 + 0.1692T$
			1723 to 1923	$-509.600 + 0.1297T$
1979	Klekamp and Supawan [11]	e.m.f./Fe + "FeO"	1070 to 1320	$-571.800 + 0.1662T$
1984	Pejryd [12]	e.m.f./air	940 to 1450	$-529.210 - 0.1268T$ $+0.0362T\ln T$
1986	O'Neill [13]	e.m.f./Fe + "FeO"	1000 to 1400	$-603.268 + 0.3375T$ $-0.0207T\ln T$
1987	Jacob *et al.* [15]	e.m.f./O_2	900 to 1500	$-578.880 + 0.1685T$
1994	Bygden *et al.* [14]	e.m.f./Fe + "FeO"	1224 to 1584	$-580.560 + 0.173T$
2007	This study	e.m.f./O_2	925 to 1533	$-579.821 + 0.170T$
		Buffer electrode	1533 to 1925	$-564.634 + 0.1601T$

the techniques used and temperature ranges covered by different investigators. Of all the previous studies listed only two spanned sufficient temperature range on either side of the transition to be able to detect it. Alcock and Chan [9] did not observe any change in slope, while Iwase *et al.* [10] detected a very large change of slope with entropy change of 39.5 $J \cdot mol^{-1} \cdot K^{-1}$ at $T = 1723$ K, but did not link it a phase transition in MoO_2.

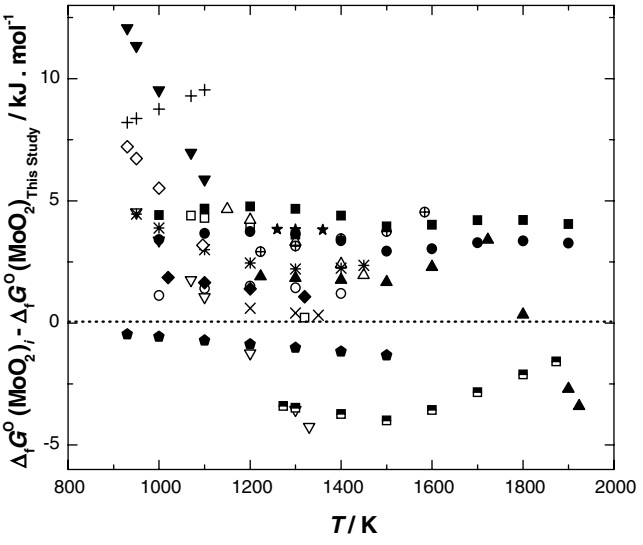

FIGURE 4. Difference between the standard Gibbs free energy of formation, $\Delta_f G^\circ(MoO_2)$, reported in the literature and that obtained in this study, as a function of temperature T: ◇, Tonosaki [1]; ▽, Gokcen [2]; ×, Gleiser and Chipman [3]; ▼, Vassilev *et al.* [4]; ◆, Rapp [5]; +, Barbi [6]; ★, Drobyshev *et al.* [7]; △, Berglund and Kierkegaard [8]; ⬒, Alcock and Chan [9]; ▲, Iwase *et al.* [10]; □, Kleykamp and Supawan [11]; ✳, Pejryd [12]; ○, O'Neill [13]; ⊕, Bygden *et al.* [14]; ⬟, Jacob *et al.* [15]; ■, JANAF (1985) [27]; and ●, Pankratz [28].

Figure 4 shows graphically the difference between the values of Gibbs free energy of formation, $\Delta_f G^\circ(MoO_{2-\delta})$, reported in the literature and that obtained in this study as a function of temperature, T/K. The difference in Gibbs free energy is plotted to provide better graphical resolution of the data. The data in the literature fall into two sets. The standard Gibbs free energy of formation reported in the majority of the studies is more positive than that obtained in this study. Thermodynamic compilations [27,28] depend on this set of data. Use of very fine powders of MoO_2 may be responsible for the more positive values. However, more negative are the results of Alcock and Chan [9], Jacob *et al.* [15]. The data of Gokcen [2] and Iwase *et al.* [10] fall on both sides: more positive at lower temperatures and more negative at higher temperatures. In the temperature range (925 to 1500) K, the results of this study are in good agreement with values of Gleiser and Chipman [3], and in fair agreement with the measurements of Rapp [5], O'Neill [13], and Jacob *et al.* [15]. It is significant that these closely agreeing results are obtained by a variety of techniques; Gleiser and Chipman [3] using the gas equilibrium method, Rapp [5] using e.m.f. method with Ni + NiO and Fe + "FeO" as reference electrodes, O'Neill [13] using the e.m.f. method with Fe + "FeO" reference and Jacob *et al.* [15] using pure O_2 gas reference. In the latter case polarization effects (gradual drift with time of the e.m.f. to lower values) were noticed, but was compensated by passing d.c. current to restore the electrode to the non-polarized state. In retrospect, the compensation may have been slightly overdone. The polarization effect is expected to be less significant when Ni + NiO and Fe + "FeO" are used as reference electrodes, since the oxygen chemical potentials associated with these solid electrodes are lower and the driving force for oxygen transport through the solid electrolyte is correspondingly reduced. The result of

Kleykamp and Supawan [11] at $T = 1323$ K agrees well with this study, but their results at lower temperatures are more positive. Since all previous e.m.f. studies were done without the buffer electrode with Mo and $MoO_{2-\delta}$ of unspecified particle size, the results obtained in this study may be considered more reliable. The data of Tonosaki [1], Vassilev *et al.* [4], and Barbi [6] are significantly more positive and may now be discarded.

The value of the nonstoichiometric parameter δ in $MoO_{2-\delta}$ has not been determined accurately. The measurements of Zador and Alcock [29] suggest a value of $(\delta \pm 0.004 = 0.01)$ at $T = 1273$ K. The results obtained by coulometric titration and thermogravimetry showed considerable difference. However, the small nonstoichiometry is unlikely to affect the value of Gibbs free energy of formation. Hence, the values obtained in this study can be tentatively considered to be identical to that of stoichiometric MoO_2 and effect of nonstoichiometry will be neglected in further discussion. The dioxide also takes up excess oxygen up to $MoO_{2.03}$ at 1273 K [29].

Since both low- and high-temperature heat capacities are available for MoO_2, the entropy is well defined. The heat capacity measurements are critically assessed in NIST-JANAF tables [27] and we are in general agreement with the entropy and heat content data up to the phase transition temperature (1533 K). The value of standard entropy is listed as $S^\circ_{298.15} = (46.459 \pm 0.42)\ \mathrm{J \cdot mol^{-1} \cdot K^{-1}}$. Third-law analysis of the high temperature Gibbs free energy data provides a convenient check of its temperature dependence. The standard enthalpy of formation at $T = 298.15$ K, $\Delta_f H^\circ_{298.15}$, can be calculated from the value of the standard Gibbs free energy of formation at each temperature, $\Delta_f G^\circ(T)$, using the following relation:

$$\Delta_f H^\circ_{298.15} = \Delta_f G^\circ(T) - \Delta(H^\circ_T - H^\circ_{298.15}) + T\{\Delta_f S^\circ_{298.15} + \Delta(S^\circ_T - S^\circ_{298.15})\}. \quad (6)$$

The values of $H^\circ_T - H^\circ_{298.15}$ and $S^\circ_T - S^\circ_{298.15}$ for monoclinic MoO_2, Mo solid, and O_2 gas along with value of $\Delta_f S^\circ_{298.15}$ were taken from NIST-JANAF [27]. The "third-law" analysis of the Gibbs free energy of formation obtained in this study in the temperature range (925 to 1533) K gives a mean value of $\Delta_f H^\circ_{298.15} = (-592.28 \pm 0.33)\ \mathrm{kJ \cdot mol^{-1}}$, with maximum variation of $0.91\ \mathrm{kJ \cdot mol^{-1}}$. The very small drift suggests that the temperature dependence of Gibbs free energy measured in this study is essentially consistent with the thermal data. The value of $\Delta_f H^\circ_{298.15}$ obtained by "third-law" analysis compares with values of $(-587.85 \pm 2.9)\ \mathrm{kJ \cdot mol^{-1}}$ recommended in NIST-JANAF [27]. It is recognized in this compilation [27] that a value more negative by $2.1\ \mathrm{kJ \cdot mol^{-1}}$ would have provided a better overall fit of all Mo–O data available at that time. Since such a revision required readjustment of data for higher oxides of molybdenum, the observation was not implemented. The value of $\Delta_f H^\circ_{298.15}$ in other compilations is $-588.94\ \mathrm{kJ \cdot mol^{-1}}$ [28,30]. A small part of the difference between calorimetric data for $\Delta_f H^\circ_{298.15}$ and that deduced from Gibbs free energy of formation may be related to nonstoichiometry. Nevertheless, the results of this study argue for a downward revision of the accepted data for $\Delta_f H^\circ_{298.15}$ and reassessment of thermal data at temperatures above the transition. In fact the assessed heat capacity in NIST-JANAF [27] deviates significantly from measurements of King *et al.* [31] at the higher temperatures: the experimental data at $T = 1801$ K was excluded from the analysis because it deviated (+2.3)% from the assessed value. The rapid increase in measured heat capacity above $T = 1500$ K is consistent with the proposed phase transition.

From the change in slope of the e.m.f. at $T = 1533$ K, the entropy of phase transition of $MoO_{2-\delta}$ is evaluated as $\Delta S_{tr} = (9.91 \pm 1.27)\ \mathrm{J \cdot mol^{-1} \cdot K^{-1}}$. The corresponding transition enthalpy change is $\Delta H_{tr} = (15.19 \pm 2.1)\ \mathrm{kJ \cdot mol^{-1}}$. Since this transition has not been reported in the literature, it warrants further discussion. The monoclinic structure of MoO_2 can be considered as a deformed rutile type [32]. In the rutile structure, each metal atom coordinates six oxygen atoms to form MO_6 octahedra. The MO_6 octahedra are joined by sharing edges to form strings. The metal–oxygen distances fall into two sets; four equal distances involved in edge-sharing in the chain, and two perpendicular to them. MoO_2 has four short and two long M–O distances. The strings are mutually connected to three-dimensional structure by octahedra having corners in common. The oxygen atom is in planar threefold coordination. In the undistorted rutile structure the metal atoms are equidistantly arranged within the strings, whereas in the MoO_2-type distorted rutile structure metal atoms are alternatively nearer to and farther from each other. The coupling or dimerization of the metal atoms leads to monoclinic symmetry.

The monoclinic distortion and the metallic property of MoO_2 have an electronic origin [33]. Of the two d electrons associated with molybdenum, one is involved in Mo–Mo bonding that distorts the otherwise tetragonal structure to monoclinic symmetry. In an octahedral crystal field, the two 4d electrons of Mo^{4+} would occupy the triply degenerate t_{2g} levels. In the rutile structure, the t_{2g} levels would be split into a nondegenerate (more stable) $t_\parallel$ and doubly degenerate $t_\perp$. The $t_\parallel$ containing one of the d electrons overlaps directly along the linear chains of the edge-shared octahedra running parallel to the rutile *c*-axis, resulting in the formation of Mo–Mo bonds (0.25 nm) within the chain. This dimerization can also be described as a type of Peierls instability [34]. The doubly degenerate $t_\perp$ overlap the π orbitals of oxygen forming Mo–O π^* bands. The second d electron of Mo^{4+} occupies the Mo–O π^* band, making MoO_2 metallic. He 1 photoelectron spectrum of MoO_2 provides direct evidence for this bonding picture: Mo–Mo bonding states are clearly resolved below the Mo–O π^* states and a sharp Fermi surface within the partially filled Mo–O π^* band [35].

Whether the rutile or MoO_2-type deformed rutile structure is adopted can be temperature dependent. The dis-

torted structures have lower entropy compared to their undistorted counterparts. When enthalpy change associated with the distortion is not too large, the structure will rid itself of the distortion at higher temperatures. For example, VO_2 (V^{4+}:$3d^1$) has the monoclinic structure below $T = 340$ (± 5) K and rutile structure (tetragonal, space group $P4_2/mnm$) above that [32]. The structure transition in VO_2 and the source of the distortion are similar to that of MoO_2, but the structure transition in VO_2 is also accompanied by a metal–insulator transition. In VO_2 the entropy change for the transition is $\Delta S_{tr} = (13.2 \pm 1.2)\ J \cdot mol^{-1} \cdot K^{-1}$ [27]. The monoclinic to tetragonal phase transition in MoO_2 (Mo^{4+}:$4d^2$) detected in this study fits this pattern. The higher transition temperature for MoO_2 is the result of stronger metal–metal bonds. It would be interesting to investigate whether WO_2 (W^{4+}:$5d^2$) and TcO_2 (Tc^{4+}:$4d^3$) which have the deformed rutile structure similar to MoO_2 at low temperature will transform to the rutile structure at higher temperatures. The transition temperature will give an indication of the strength of metal–metal bonding along the edge-sharing chains of MO_6 octahedra.

4. Conclusion

New high-temperature solid-state electrochemical measurements using an advanced cell design have generated accurate data on the standard Gibbs free energy of formation of $MoO_{2-\delta}$ in two crystallographic forms, monoclinic and tetragonal. The standard Gibbs free energy of formation of monoclinic phase of MoO_2 is: $\Delta_f G^\circ(MoO_{2-\delta}) \pm 570/(J \cdot mol^{-1}) = -579{,}821 + 170.003\,(T/K)$ in the temperature range (925 to 1533) K. The standard Gibbs free energy of formation of tetragonal phase is: $\Delta_f G^\circ(MoO_{2-\delta}) \pm 510/(J \cdot mol^{-1}) = -564{,}634 + 160.096(T/K)$ in the temperature range (1533 to 1925) K. The new measurements on microcrystalline $MoO_{2-\delta}$ improve thermodynamic data for MoO_2 and suggest a value of $\Delta_f H^\circ_{298.15}(MoO_2) = (-592.28 \pm 0.33)$ $kJ \cdot mol^{-1}$, (3 to 4) $kJ \cdot mol^{-1}$ more negative than values given in thermodynamic compilations. Accurate measurements on the nonstoichiometry of MoO_2 as a function of temperature will help to further refine the data for this compound.

Identified in this study is a hitherto undetected phase transition in MoO_2 at $T = 1533$ K from deformed-rutile to rutile structure. The entropy of this phase transition is obtained as $\Delta S_{tr} = (9.91 \pm 1.27)\ J \cdot mol^{-1} \cdot K^{-1}$. The nature of chemical bond that gives rise to the structure distortion at lower temperatures and entropy stabilization of the undistorted structure at high temperatures are discussed in comparison with an analogous system.

Acknowledgements

One of the authors (J.G.) thanks the Department of Science and Technology, Government of India for the award of Ramanna Fellowship.

References

[1] K. Tonosaki, Bull. Inst. Phys. Chem. Res. Jpn. 19 (1940) 126–132.
[2] N.A. Gokcen, J. Met. 197 (1953) 1019–1020.
[3] M. Gleiser, J. Chipman, J. Phys. Chem. 66 (1962) 1539–1540.
[4] C. Vassilev, T. Nikolov, M. Chimbulev, Trans. Inst. Min. Metall. 77 (1968) C36–C38.
[5] R.A. Rapp, Trans. Metall. Soc. AIME 227 (1963) 371–374.
[6] G.B. Barbi, J. Phys. Chem. 68 (1964) 1025–1029.
[7] V.N. Drobyshev, T.N. Rezukhina, L.A. Tarasova, Russ. J. Phys. Chem. 39 (1965) 70–73.
[8] S. Berglund, P. Kierkegaard, Acta Chem. Scand. 23 (1969) 329–330.
[9] C.B. Alcock, J.C. Chan, Can. Metall. Quart. 11 (1972) 559–567.
[10] M. Iwase, M. Yasuda, T. Mori, Electrochim. Acta 24 (1979) 261–266.
[11] H. Kleykamp, A. Supawan, J. Less Comm. Met. 63 (1979) 237–244.
[12] L. Pejryd, High Temp.-High Press. 16 (1984) 403–408.
[13] H.St.C. O'Neill, Am. Mineral. 71 (1986) 1007–1010.
[14] J. Bygden, D. Sichen, S. Seetharaman, Metall. Mater. Trans. B 25 (1994) 885–891.
[15] K.T. Jacob, G.M. Kale, G.N.K. Iyengar, J. Mater. Sci. 22 (1987) 4274–4280.
[16] K.T. Jacob, K.P. Jayadevan, R.M. Mallya, Y. Waseda, Adv. Mater. 12 (2000) 440–444.
[17] K.T. Jacob, T. Mathews, Indian J. Technol. 28 (1990) 413–427.
[18] J.N. Pratt, Metall. Trans. A 21 (1990) 1223–1250.
[19] J. Fouletier, P. Fabry, M. Kleitz, J. Electrochem. Soc. 123 (1976) 204–213.
[20] G.G. Charette, S.N. Flengas, J. Electrochem. Soc. 115 (1968) 796–804.
[21] G.M. Kale, K.T. Jacob, Metall. Trans. B 23 (1992) 57–64.
[22] K.T. Jacob, T.H. Okabe, T. Uda, Y. Waseda, J. Phase Equilibr. 20 (1999) 553–564.
[23] K.T. Jacob, T.H. Okabe, T. Uda, Y. Waseda, Mater. Sci. Eng. B 64 (1999) 44–53.
[24] K.T. Jacob, Metall. Trans. B 17B (1986) 763–769.
[25] K.T. Jacob, S.S. Pandit, Steel Res. 58 (1987) 105–110.
[26] K.T. Jacob, C. Sekhar, Y. Waseda, J. Am. Ceram. Soc. (accepted for publication).
[27] M.W. Chase Jr. (Ed.), NIST-JANAF Thermochemical Tables, 4th ed., J. Phys. Chem. Ref. Data, Monograph No. 9, American Institute of Physics, USA, 1998, p. 1585.
[28] L.B. Pankratz, Thermodynamic Properties of Elements and Oxides, United States Department of the Interior, Bureau of Mines, Bulletin 672, 1982.
[29] S. Zador, C.B. Alcock, J. Chem. Thermodyn. 2 (1970) 9–16.
[30] I. Barin, Thermochemical Data of Pure Substances, second ed., VCH, Weinheim, 1993.
[31] E.G. King, W.W. Weller, A.U. Christensen, US Bur. Mines, RI 5664, 1960.
[32] A. Magneli, G. Anderson, Acta Chem. Scand. 9 (1955) 1378–1381.
[33] D.B. Rogers, R.D. Shannon, A.W. Sleight, J.L. Gilson, Inorg. Chem. 8 (1969) 841–847.
[34] V. Eyert, R. Horny, K.-H. Höck, S. Horn, J. Phys. 12 (2000) 4923–4946.
[35] F. Werfel, E. Minni, J. Phys. C 16 (1983) 6091–6100.

JCT 07-173